

Forced Oscillation Source Location of Bulk Power Systems Using Synchrosqueezing Wavelet Transform

Tao Jiang, *Senior Member, IEEE*, Bohan Liu, Guodong Liu, *Senior Member, IEEE*,
Bin Wang, *Senior Member, IEEE*, Xue Li, *Member*, Jinan Zhang

1

Abstract—Forced oscillation source location (FOSL) plays a significant role in mitigating forced oscillations (FOs), which threaten the power system stability. This paper proposes a data-driven approach for FOSL in power systems using synchrosqueezing wavelet transform (SWT). The proposed approach conducts SWT on the measured system responses to obtain the SWT matrix. Then, the SWT-based dissipating energy flow (DEF) model in time-frequency domain and dissipating energy spectrum (DES) model in frequency domain are derived from the traditional DEF model. Further, the characteristics of SWT-based DEF and DES are revealed by referring to the traditional DEF, and the FOSL criteria of the SWT-based DEF and DES can be hereby obtained. Using the obtained FOSL criteria, the FO source can be located from the measured responses. The performance of the proposed FOSL method is evaluated by simulation data of the WECC 179-bus test system and field-measurement PMU data of the ISO New England, the results confirm the accuracy and efficiency of the proposed method in the FOSL.

Index Terms—forced oscillation, oscillation source location, synchrosqueezing wavelet transform, dissipating energy flow.

NOMENCLATURE

<i>CWT</i>	Continuous wavelet transform.
<i>DEF</i>	Dissipating energy flow.
<i>DES</i>	Dissipating energy spectrum.
<i>FO</i>	Forced oscillation.
<i>FOSL</i>	Forced oscillation source location.
<i>FSST</i>	Short-time Fourier transform based synchrosqueezing transform.
<i>IMF</i>	Intrinsic mode functions.
<i>MEMD</i>	Multivariate empirical mode decomposition.
<i>PMU</i>	Phasor measurement unit.
<i>STFT</i>	Short-time Fourier transform.
<i>SWT</i>	Synchrosqueezing wavelet transform.
<i>TEO</i>	Teager energy operator.
<i>WAMS</i>	Wide area measurement system.
<i>WECC</i>	Western Electricity Coordinating Council.

The authors would like to thank the support in part by National Natural Science Foundation of China (Grant No. U2066208, 51877033, 52077028).

Tao Jiang, Bohan Liu and Xue Li are with the Department of Electrical Engineering, Northeast Electric Power University, Jilin, JL 132012 China.

Guodong Liu is with the Oak Ridge National Laboratory, Oak Ridge, TN 37831, USA.

Bin Wang is with the Department of ECE, University of Texas, San Antonio, TX 78249, USA.

Jinan Zhang is with the College of Engineering, University of Georgia, Athens, GA, 30602, USA.

I. INTRODUCTION

In recent years, forced oscillations (FOs) have been reported frequently in power grids, which seriously threaten the security and stability of power systems [1]-[2]. In May 2013, an FO occurred in China Southern Power Grid led to generator tripping, eventually [3]. In January 2018, an FO with an oscillation frequency of 1.57Hz occurred in the New England, resulting in significant power oscillations on the interconnections [4]. In March 2018, an FO occurred in the Indian power grid, which lasted for about 5 minutes, led to large oscillations of bus voltage in several substations [5]. The reports of these events also highlight the effectiveness of fast isolating FO sources as a means to mitigate the FO. Therefore, it is of great significance to locate the FO source quickly and accurately to mitigate the FO in power systems [6].

To locate the FO sources efficiently, lots of efforts have been made. In [7], the statistical signatures of FO source including the kurtosis and the power spectral density were explored to locate the oscillation sources using the phasor measurement units (PMUs) data. In [8], the energy injected into the generator was decomposed into the energy of the governor system and the energy of the excitation system, and then the FO source was located on the control system of the generator. In [9], a machine learning based time-series classification method was presented to distinguish the FO source using synchrophasor measurements. In [10], a deep learning-based FOSL approach is presented for bulk power systems. In [11], dissipating energy flow (DEF) was proposed to locate the FO source, and the generator injecting dissipating energy to power grid was located as the FO source. In [12], an extension of DEF was developed using a complex integral approach. Among the above methods, DEF has shown promising results in the real-world power grids due to its computational efficiency and location accuracy [13]-[15].

Although the DEF has been demonstrated as an effective method for locating FOSL, its performance is subjected to the extracted FO components from the measurements [16]-[19]. To address this issue, a short-time Fourier transform (STFT) based dissipating energy spectrum (DES) derived from DEF was proposed in [16] to identify the FO source in frequency-domain. In [17], STFT-based synchrosqueezing transform (FSST) was proposed to calculate the DEF by using the extracted FSST coefficients associated with FO mode from the measurements. In [18], a time-scale domain FOSL method, which converts the DEF from time domain to time-scale domain, was proposed based on Continuous Wavelet Transform (CWT). In [19], multivariate empirical mode decomposition (MEMD) and Teager energy operator (TEO)

were used to calculate the DEF by separating the FO components from the multi-channel measurements. Although, the above methods can effectively extract the FO components from the measurements and locate the FO sources, the solution process is cumbersome, and the calculation efficiency is low. In addition, the PMU measurement channels are seriously affected by the observability of FO modes, leading to frequencies fluctuates in the FO components from different channels. This variation also potentially affects the accuracy of FOSL.

To bridge the gaps above, this paper proposed an SWT-based method for power system FOSL. The measurements collected from the PMUs in power systems are decomposed by SWT. Then, the SWT-based DEF in time-frequency domain and DES in frequency domain are derived separately. For FO source and FO sink, the characteristics of DEF in time-frequency domain and DES in frequency domain are revealed. According to the revealed characteristics of DEF and DES, the FO source is determined. The main contributions of this paper are:

1. The proposed SWT-based method does not require the reconstruction of the time-domain FO component and directly locates the FO source in the time-frequency domain and frequency domain using the SWT coefficients.

2. In time-frequency domain, FO is concentrated by the proposed SWT-based method, overcoming the scale blurred representation encountered in the conventional CWT.

3. By leveraging abrupt change of DES in frequency domain, the proposed method efficiently locates FO source without requiring pre-determined FO frequency.

4. Referring to the criteria of FOSL using DEF in time domain, the characteristics of DEF in both the time-frequency and frequency domain are fully discussed and validated in this paper.

The rest of this paper is organized as follows. In Section II, the general DEF and SWT are introduced. In Section III, the proposed SWT-based FOSL in time-frequency and frequency domains are presented. In Section IV, the proposed FOSL is validated using simulation data of the WECC 179-bus test system and the field-measurement PMU data from the ISO New England. Finally, conclusions are drawn in Section V.

II. THEORETICAL BACKGROUND

A. Dissipating Energy Flow

In power systems, the FO typically accompanies with oscillation energy exchange. During the FO, the FO source continuously injects energy into the power grid. According to the energy exchange characteristic of the FO, a DEF method was proposed in [14] to trace the FO source using the measured responses, the DEF flowing into bus j through branch L_{ij} was defined as

$$W_j^D = \int (\Delta P_{ij} d\Delta\theta_j + \Delta Q_{ij} d(\Delta \ln U_j)) \quad (1)$$

$$= \int (\Delta P_{ij} 2\pi \Delta f_j dt + \Delta Q_{ij} d(\Delta \ln U_j))$$

where, ΔP_{ij} and ΔQ_{ij} are the active and reactive power variation on branch L_{ij} , $\Delta\theta_j$ is the voltage angle variation at bus j , $\Delta \ln U_j$ is the logarithmic variation of the voltage magnitude at bus j , Δf_j is the frequency variation at bus j .

The criteria of FOSL based on DEF in time domain are summarized as follows [11]: If the DEF at FO frequency is negative and its trend is downward, it indicates that there is dynamic component(s) behind bus j continuously injecting energy into the power grid, thus could be identified as an FO source. If the DEF at FO frequency is positive and its trend is upward, it indicates that there is dynamic component(s) behind bus j continuously absorbing energy from the power grid, thus could be identified as an FO sink. In the practical application of DEF, it is necessary to estimate the FO frequency by FFT and extract the FO component from the measurements to improve the accuracy of FOSL.

B. Synchrosqueezing wavelet transform (SWT)

Although the DEF can be used to locate the FO source, its performance is subjected to the FO component extracted from the measurements. Several signal processing methods are adopted to separate the FO components from the measured responses, such as CWT [18], band-pass filtering (BF) [20], EMD [21], etc. However, BF can introduce signal distortion near the cutoff frequency, EMD suffers from mode mixing issues, and CWT exhibits scale blurred representation. To deal with the above shortcomings, SWT is proposed in this section to extract the FO components from the measured responses.

SWT is a powerful signal processing technique that reassigns CWT coefficients to accurately localize the oscillation components of the signal, enhancing the frequency resolution and coping with the scale blurred representation of the CWT.

Taking the variation of active power $\Delta P_{ij}(t)$ as an example, its corresponding CWT coefficients is [22]

$$\mathfrak{R}_{\Delta P}(c, \tau) = \frac{1}{\sqrt{c}} \int_{-\infty}^{+\infty} \Delta P_{ij}(t) \psi^* \left(\frac{t-\tau}{c} \right) dt \quad (2)$$

where $\mathfrak{R}_{\Delta P}(c, \tau)$ is the CWT coefficient of $\Delta P_{ij}(t)$. ψ is the wavelet. c is the scale factor. τ is the translation factor. The superscript “*” represents a conjugate operation.

To obtain the FO component in the time domain, an inverse wavelet transform is performed at the critical scale factor c_r associated with the FO frequency.

$$\Delta P_{ij,r}(t) = \frac{1}{C_\phi} \iint \mathfrak{R}_{\Delta P,r}(c, \tau) \psi \left(\frac{t-\tau}{c} \right) \frac{dc d\tau}{|c|} \quad (3)$$

where $\Delta P_{ij,r}(t)$ is the FO component contained in $\Delta P_{ij}(t)$, C_ϕ is the wavelet admissible constant and expressed as

$$C_\phi = \int_0^{+\infty} \frac{|\hat{\psi}(\omega)|^2}{\omega} d\omega < +\infty \quad (4)$$

where $\hat{\psi}(\omega)$ is the Fourier transform of wavelet function $\psi(t)$.

For any point (c, τ) in the time-scale domain, its instantaneous angular frequency $\omega_{\Delta P}(c, \tau)$ is [23]

$$\omega_{\Delta P}(c, \tau) = \frac{-i}{\mathfrak{R}_{\Delta P}(c, \tau)} \frac{\partial \mathfrak{R}_{\Delta P}(c, \tau)}{\partial \tau} \quad (5)$$

After obtaining the instantaneous angular frequency, the CWT coefficients with scale blurred near the FO frequency ω_k are squeezed, and the CWT coefficients originally distributed in the time-scale domain can be transformed into SWT coefficients $T_{\Delta P}(\omega_k, \tau)$

$$T_{\Delta P}(\omega_k, \tau) = \int_{c_{r-\mu}}^{c_{r+\mu}} \mathfrak{R}_{\Delta P}(c, \tau) \Delta \omega \frac{dc}{c} \quad (6)$$

where c_r is the wavelet scale corresponding to the FO frequency ω_k . $\Delta\omega = \omega_k - \omega_{k-1}$. Interval $[c_{r-\mu}, c_{r+\nu}]$ is the upper and lower limits of scale blurred representation with corresponding frequency range $[\omega_k - \Delta\omega/2, \omega_k + \Delta\omega/2]$. The corresponding relationship between the integral upper and lower limits of scale factor and frequency in (6) can be obtained by (5). In (6), the CWT coefficients in $[c_{r-\mu}, c_{r+\nu}]$ can be squeezed into SWT coefficients with a center frequency at ω_k .

According to (6), the SWT coefficient matrix of $\Delta P_{ij}(t)$ can be expressed as

$$\mathbf{T}_{\Delta P} = \begin{bmatrix} \mathbf{T}_{\Delta P}(\omega_1, \tau) \\ \mathbf{T}_{\Delta P}(\omega_2, \tau) \\ \mathbf{M} \\ \mathbf{T}_{\Delta P}(\omega_k, \tau) \\ \mathbf{M} \\ \mathbf{T}_{\Delta P}(\omega_z, \tau) \end{bmatrix} = \begin{bmatrix} T_{\Delta P}(\omega_1, \tau_1) & T_{\Delta P}(\omega_1, \tau_2) & \text{L} & T_{\Delta P}(\omega_1, \tau_n) \\ T_{\Delta P}(\omega_2, \tau_1) & T_{\Delta P}(\omega_2, \tau_2) & \text{L} & T_{\Delta P}(\omega_2, \tau_n) \\ \mathbf{M} & \mathbf{M} & \mathbf{O} & \mathbf{M} \\ T_{\Delta P}(\omega_k, \tau_1) & T_{\Delta P}(\omega_k, \tau_2) & \text{L} & T_{\Delta P}(\omega_k, \tau_n) \\ \mathbf{M} & \mathbf{M} & \mathbf{O} & \mathbf{M} \\ T_{\Delta P}(\omega_z, \tau_1) & T_{\Delta P}(\omega_z, \tau_2) & \text{L} & T_{\Delta P}(\omega_z, \tau_n) \end{bmatrix} \quad (7)$$

where, $\mathbf{T}_{\Delta P}$ is the SWT coefficient matrix of $\Delta P_{ij}(t)$, $\mathbf{T}_{\Delta P}(\omega_z, \tau)$ is the SWT coefficient vector of $\Delta P_{ij}(t)$ at ω_z , $T_{\Delta P}(\omega_k, \tau_n)$ is the SWT coefficient of $\Delta P_{ij}(t)$ at ω_z with τ_n .

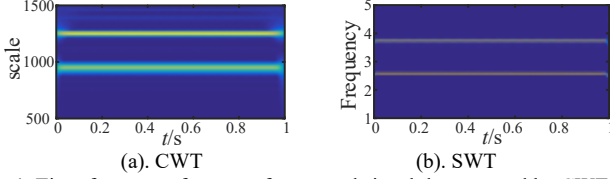


Fig. 1. Time-frequency features of measured signal decomposed by CWT and SWT

Taking $\Delta P_{ij}(t)$ with two FO modes as an example, Fig. 1 shows the curves in the time-frequency domain decomposed by CWT and SWT, separately. It can be observed that the wavelet scales associated with the FO modes exhibit significant fluctuations in wavelet scale intervals, resulting in a serious scale blurred representation. However, the time-frequency curves decomposed by SWT are concentrated at the FO frequencies, effectively avoiding the scale blurred representation of CWT.

Further, the FO component in the time domain can be obtained by using the inverse transformation on $\mathbf{T}_{\Delta P}(\omega_k, \tau)$

$$\Delta P_{ij,k}(t) = 2\text{Re} \left(\frac{1}{C_\varphi} \int_{\omega_k - \Delta\omega/2}^{\omega_k + \Delta\omega/2} \mathbf{T}_{\Delta P}(\omega_k, \tau) d\omega \right) \quad (8)$$

where, $\text{Re}(\bullet)$ is the real part of the complex number.

To extract the $\mathbf{T}_{\Delta P}(\omega_k, \tau)$ associated with FO mode in (8) from the SWT coefficient matrix (7), the relative energy weight is adopted

$$H(k) = \frac{\sum_{v=1}^n |T_{\Delta P}(\omega_k, \tau_v)|}{\sum_{k=1}^z \sum_{v=1}^n |T_{\Delta P}(\omega_k, \tau_v)|} \quad (9)$$

where, $H(k)$ is the relative energy weight at the k th angular frequency, z is the row number of the coefficient matrix $\mathbf{T}_{\Delta P}$, while n is the column number.

If the $H(k)$ in (9) is greater than the energy weight threshold H_0 , then ω_k can be considered as the FO frequency and the $\mathbf{T}_{\Delta P}(\omega_k, \tau)$ can be distinguished as the SWT coefficient vector of the FO mode. Selection of H_0 plays a crucial role in extracting the SWT coefficient vector associated with FO

mode. A larger H_0 may result in missing the dominant SWT coefficient vectors, while a smaller H_0 may include irrelevant SWT coefficient vectors. To ensure the separation accuracy of FO mode, a typical setting of the threshold H_0 of relative energy weight is 0.1, and its performance will be verified in the appendix.

III. PROPOSED METHODOLOGY

This section presents the definitions and derivations of the DEF in time-frequency domain and the DES in frequency domain using the SWT. The FOSL criteria of the proposed DEF in time-frequency domain and the DES in frequency are presented.

A. FOSL method in Time-Frequency Domain

According to the inner product of CWT [24], the integral of the product of $\Delta P_{ij}(t)$ and $\Delta f_j(t)$ in (1) can be represented as

$$\int \Delta P_{ij}(t) \Delta f_j(t) dt = \frac{1}{C_\varphi} \iint \Re_{\Delta P}(c_r, \tau) \Re_{\Delta f}^*(c_r, \tau) \frac{dc d\tau}{c_r^2} \quad (10)$$

where, $\Re_{\Delta P}(c_r, \tau)$ and $\Re_{\Delta f}(c_r, \tau)$ are the key wavelet coefficients of ΔP_{ij} and Δf_j that contain the FO mode, separately.

Similarly, the integral of the product of $\Delta Q_{ij}(t)$ and $\Delta \ln U_j(t)$ can be represented as

$$\int \Delta Q_{ij}(t) \Delta \ln U_j(t) dt = \frac{1}{C_\varphi} \iint \Re_{\Delta Q}(c_r, \tau) \Re_{\Delta \ln U}^*(c_r, \tau) \frac{dc d\tau}{c_r^2} \quad (11)$$

where, $\Re_{\Delta Q}(c_r, \tau)$ and $\Re_{\Delta \ln U}(c_r, \tau)$ are the critical wavelet coefficients of ΔQ_{ij} and $\Delta \ln U$ associated with the FO mode, separately.

By substituting (10) and (11) into (1), the CWT-based DEF from bus j in time-frequency domain can be expressed as

$$E_{j,\text{CWT}}^D = \frac{2\pi}{C_\varphi} \iint (\Re_{\Delta P}(c_r, \tau) \Re_{\Delta f}^*(c_r, \tau)) \frac{dc d\tau}{c_r^2} + \frac{1}{C_\varphi} \iint (\Re_{\Delta Q}(c_r, \tau) \Re_{\Delta \ln U}^*(c_r, \tau)) \frac{dc d\tau}{c_r^2} \quad (12)$$

Due to the observability of the FO mode, the critical wavelet scale associated with FO mode fluctuates within the wavelet scale interval $[c_{r-\alpha}, c_{r+\beta}]$. As observed in Fig. 1, there is a scale blurred representation decomposed by the CWT. To avoid the influence of the observability of the FO mode and the scale blurred representation on the computational accuracy of the DEF in time-scale domain, the SWT-based method is used. Based on derivation of SWT in Eq. (6), $E_{j,\text{CWT}}^D$ in (12) is integrated in the wavelet scale interval $[c_{r-\alpha}, c_{r+\beta}]$. The above process can be expressed as:

$$\int_{c_{r-\alpha}}^{c_{r+\beta}} E_{j,\text{CWT}}^D dc = \frac{2\pi}{C_\varphi} \int_{c_{r-\alpha}}^{c_{r+\beta}} \int_{c_{r-\alpha}}^{c_{r+\beta}} (\Re_{\Delta P}(c_r, \tau) \Re_{\Delta f}^*(c_r, \tau)) \frac{dc d\tau}{C_\varphi c_r^2} dc + \frac{1}{C_\varphi} \int_{c_{r-\alpha}}^{c_{r+\beta}} \int_{c_{r-\alpha}}^{c_{r+\beta}} (\Re_{\Delta Q}(c_r, \tau) \Re_{\Delta \ln U}^*(c_r, \tau)) \frac{dc d\tau}{C_\varphi c_r^2} dc \quad (13)$$

where, $\int_{c_{r-\alpha}}^{c_{r+\beta}} E_{j,\text{CWT}}^D dc$ is the integration of DEF in the wavelet scale interval $[c_{r-\alpha}, c_{r+\beta}]$.

Let $\int_{c_{r-\alpha}}^{c_{r+\beta}} E_{j,\text{CWT}}^D dc = E_{j,\text{SWT}}^D$. Then, (13) could be derived as

$$\begin{aligned}
E_{j,\text{SWT}}^D &= \frac{2\pi}{\Delta^2 \omega C_\phi} \int \left(\int_{c_{r-a}}^{c_{r+\beta}} \Re_{\Delta P}(c_r, \tau) \Delta \omega \frac{dc}{c_r} \right) \times \left(\int_{c_{r-a}}^{c_{r+\beta}} \Re_{\Delta f}^*(c_r, \tau) \Delta \omega \frac{dc}{c_r} \right) d\tau \\
&+ \frac{1}{\Delta^2 \omega C_\phi} \int \left(\int_{c_{r-a}}^{c_{r+\beta}} \Re_{\Delta Q}(c_r, \tau) \Delta \omega \frac{dc}{c_r} \right) \times \left(\int_{c_{r-a}}^{c_{r+\beta}} \Re_{\Delta \ln U}^*(c_r, \tau) \Delta \omega \frac{dc}{c_r} \right) d\tau \\
&= \frac{2\pi}{\Delta^2 \omega C_\phi} \int (T_{\Delta P}(\omega_k, \tau) T_{\Delta f}^*(\omega_k, \tau)) d\tau \\
&+ \frac{1}{\Delta^2 \omega C_\phi} \int (T_{\Delta Q}(\omega_k, \tau) T_{\Delta \ln U}^*(\omega_k, \tau)) d\tau \\
&= \frac{1}{\Delta^2 \omega C_\phi} \int (2\pi \Im_{\Delta P, \Delta f}(\omega_k, \tau) + \Im_{\Delta Q, \Delta \ln U}(\omega_k, \tau)) d\tau
\end{aligned} \tag{14}$$

where, $ED j, \text{SWT}$ is the SWT-based DEF in time-frequency domain of bus j in the wavelet scale interval $[c_{r-a}, c_{r+\beta}]$, which, in essence, is the accumulation of $ED j, \text{CWT}$ in the wavelet scale interval $[c_{r-a}, c_{r+\beta}]$. $T_{\Delta P}(\omega_k, \tau)$, $T_{\Delta f}(\omega_k, \tau)$, $T_{\Delta Q}(\omega_k, \tau)$, and $T_{\Delta \ln U}(\omega_k, \tau)$ are the SWT coefficients of ΔP_{ij} , Δf_j , ΔQ_{ij} , and $\Delta \ln U$ at the FO frequency, respectively. $\Im_{\Delta P, \Delta f}(\omega_k, \tau)$ is the mutual SWT coefficient of ΔP_{ij} and Δf_j ; $\Im_{\Delta Q, \Delta \ln U}(\omega_k, \tau)$ is the mutual SWT coefficient of ΔQ_{ij} and $\Delta \ln U$.

The observability of the FO mode causes the fluctuation of wavelet scales characterizing the FO frequency within a finite neighborhood around the key wavelet scale c_r . This leads to poor robustness in the calculation of $ED j, \text{CWT}$ in (12). Meanwhile, the solution accuracy is also affected by the observability of the FO mode. However, compared to Eq. (12), the proposed SWT-based DEF in time-frequency domain $ED j, \text{SWT}$ in (14) accumulates $ED j, \text{CWT}$ in the wavelet scale interval $[c_{r-a}, c_{r+\beta}]$, avoids the influence of the observability of FO mode on the calculation results, and ensures strong robustness of the solution. Moreover, due to the observability of the FO mode, the fluctuation interval of the wavelet scale in (14) is usually larger than the scale blurred representation interval of (6), i.e., $[c_{r-\mu}, c_{r+\nu}] \subseteq [c_{r-a}, c_{r+\beta}]$. Therefore, the proposed method not only avoids the influence of the observability of FO mode, but also solves the issue of scale blurred representation when decomposing the FO component using CWT.

Note that the proposed SWT-based DEF in time-frequency domain is derived from the DEF in the time domain by using SWT. Hence, the FOSL criteria for the DEF in time domain also can be suitable for the proposed DEF in time-frequency domain. Therefore, if the $ED j, \text{SWT}$ in time-frequency domain is negative and shows a downward trend, it indicates that the component behind bus j continuously injects energy into the power grid during the FO, the component can hereby be identified as an FO source. If the $ED j, \text{SWT}$ in time-frequency domain is positive and shows an upward trend, the component could be identified as an FO sink.

B. FOSL method in Frequency Domain

Prior to using the proposed DEF in time-frequency domain, the determination of the dominant FO frequency is still required. In addition, considering the correspondence between SWT coefficients and oscillation frequency, this section extends the DEF in time-frequency domain to frequency domain. The method directly locates the FO source through the abrupt changes of DEF in the frequency domain without prior determination of the FO frequency.

In (12), the integration of $ED j, \text{CWT}$ is calculated in the time domain, and the dissipating energy in the scale domain based on CWT can be expressed as:

$$M_{j,\text{CWT}}^D(c) = \frac{2\pi}{C_\phi} \int \Re_{\Delta P}(c_r) \Re_{\Delta f}^*(c_r) \frac{dc}{c_r^2} + \frac{1}{C_\phi} \int \Re_{\Delta Q}(c_r) \Re_{\Delta \ln U}^*(c_r) \frac{dc}{c_r^2} \tag{15}$$

where $MD j, \text{CWT}(c)$ is the wavelet dissipating energy of bus j at the wavelet scale c in the frequency domain. Similarly, to address the scale blurred representation of the CWT and improve the observability of the FO mode, the CWT-based DES in (15) is further transformed into the frequency domain, which could be expressed as

$$\begin{aligned}
\int_{c_{r-a}}^{c_{r+\beta}} M_{j,\text{CWT}}^D(c) dc &= \frac{2\pi}{C_\phi} \int_{c_{r-a}}^{c_{r+\beta}} \int_{c_{r-a}}^{c_{r+\beta}} \Re_{\Delta P}(c_r) \Re_{\Delta f}^*(c_r) \frac{dc}{c_r^2} dc \\
&+ \frac{1}{C_\phi} \int_{c_{r-a}}^{c_{r+\beta}} \int_{c_{r-a}}^{c_{r+\beta}} \Re_{\Delta Q}(c_r) \Re_{\Delta \ln U}^*(c_r) \frac{dc}{c_r^2} dc
\end{aligned} \tag{16}$$

Similar as (14), (16) can be further transformed into

$$\begin{aligned}
M_{j,\text{SWT}}^D &= \frac{2\pi}{\Delta^2 \omega C_\phi} \left(\int_{c_{r-a}}^{c_{r+\beta}} \Re_{\Delta P}(c_r) \Delta \omega \frac{dc}{c_r} \right) \times \left(\int_{c_{r-a}}^{c_{r+\beta}} \Re_{\Delta f}^*(c_r) \Delta \omega \frac{dc}{c_r} \right) \\
&+ \frac{1}{\Delta^2 \omega C_\phi} \left(\int_{c_{r-a}}^{c_{r+\beta}} \Re_{\Delta Q}(c_r) \Delta \omega \frac{dc}{c_r} \right) \times \left(\int_{c_{r-a}}^{c_{r+\beta}} \Re_{\Delta \ln U}^*(c_r) \Delta \omega \frac{dc}{c_r} \right) \\
&= \frac{1}{\Delta^2 \omega C_\phi} (2\pi T_{\Delta P}(\omega_k) T_{\Delta f}^*(\omega_k) + T_{\Delta Q}(\omega_k) T_{\Delta \ln U}^*(\omega_k)) \\
&= \frac{1}{\Delta^2 \omega C_\phi} 2\pi \wp_{\Delta P, \Delta f}(\omega_k) + \wp_{\Delta Q, \Delta \ln U}(\omega_k)
\end{aligned} \tag{17}$$

where, $MD j, \text{SWT}$ is the SWT-based frequency-domain DES of bus j in the wavelet scale interval $[c_{r-a}, c_{r+\beta}]$. Essentially, this is the accumulation of $MD j, \text{CWT}$ in the wavelet scale interval $[c_{r-a}, c_{r+\beta}]$. $T_{\Delta P}(\omega_k)$, $T_{\Delta f}(\omega_k)$, $T_{\Delta Q}(\omega_k)$, $T_{\Delta \ln U}(\omega_k)$ are the frequency domain forms of SWT coefficients of ΔP_{ij} , Δf_j , ΔQ_{ij} and $\Delta \ln U$, respectively. $\wp_{\Delta P, \Delta f}(\omega_k)$ is the mutual SWT-based energy spectral density of ΔP_{ij} and Δf_j , while $\wp_{\Delta Q, \Delta \ln U}(\omega_k)$ is the mutual SWT-based energy spectral density of ΔQ_{ij} and $\Delta \ln U$.

As discussed in the previous subsection, the FO typically fluctuates in a finite neighborhood around the key wavelet scale c_r . This introduces the challenges to the robustness and accuracy of the $MD j, \text{CWT}$ calculation in (15). To address this issue, a frequency-domain DES method is proposed, $MD j, \text{SWT}$, as shown in (17). The comparison between (15) and (17) reveals that the scale domain DES $MD j, \text{CWT}$ only characterizes the dissipating energy spectrum at the key wavelet scale c_r . In contrast, the proposed frequency domain DES $MD j, \text{SWT}$ in (17) aggregates the scale domain DES $MD j, \text{CWT}$ over the wavelet scale interval $[c_{r-a}, c_{r+\beta}]$, resulting in higher computational accuracy of DES in the frequency domain. Meanwhile, due to the observability of the FO mode, the fluctuation interval of the wavelet scale in (17) is usually larger than the scale blurred representation interval in (6), i.e., $[c_{r-\mu}, c_{r+\nu}] \subseteq [c_{r-a}, c_{r+\beta}]$. Therefore, the proposed method addresses the observability issue of the FO mode with high frequency resolution, overcoming the scale blurred representation problem in the CWT-based method.

The proposed frequency-domain DES $MD j, \text{SWT}$ is essentially derived by using SWT to map the time-domain DEF into the frequency domain, and extending the FOSL

criteria in time domain DEF into the proposed SWT-based DES. According to the spectral characteristics of the signal in [25], if the signal spectrum has a peak or valley at a particular frequency, it suggests that energy is concentrated at this frequency, making it the dominant oscillation frequency of the signal. Extending this concept to the SWT-based DES, when the SWT-based DES has a peak or valley at a particular frequency, it indicates that this frequency is the FO frequency of the system, and the corresponding oscillation mode is the FO mode. Then, the SWT-based DES at FO frequency can be used to locate the FO source.

To summarize, the proposed criteria using the SWT-based DES are as follows: If the $MD_{j,SWT}$ is negative and has the largest absolute value at the FO frequency, it indicates that the dynamic component(s) behind bus j continuously injects energy into the power grid, therefore, is the FO source. On the other hand, if the $MD_{j,SWT}$ is positive, it means that the dynamic component(s) behind bus j continuously absorbs energy from the power grid, therefore, is an FO sink.

C. Scheme of Proposed Methodology

The steps of the proposed FOSL methodology are described as follows:

Step1: Collect active power, reactive power, voltage, and frequency measurements from PMUs.

Step2: Calculate the variation of active power, reactive power, voltage, and frequency measurements.

Step3: Apply SWT to each electrical variation and obtain the SWT coefficient matrix of each electrical variation.

Step4: Calculate the relative energy weight of the electrical parameters of each bus by (9) and determine the FO frequency. The SWT coefficients of each electrical parameters at the FO frequency are extracted. Then, the SWT-based DEF $ED_{j,SWT}$ in time-frequency domain is calculated by (14).

Step5: Calculate the SWT-based DES $MD_{j,SWT}$ at each frequency by (17). According to the changing trend of $MD_{j,SWT}$ at each frequency, the FO frequency is determined, and the $MD_{j,SWT}$ at FO frequency can be obtained.

Step6: Locate the FO source in time-frequency domain and frequency domain by using the corresponding criteria proposed in subsections III-A and III-B.

IV. CASE STUDIES

In this section, the performances of the proposed FOSL in time-frequency and frequency domains are evaluated by the simulation data of the WECC 179-bus test system and the field-measurements acquired from the PMUs in ISO New England.

TABLE I
RENUMBER OF THE GENERATOR BUSES

Bus	Generator	Bus	Generator	Bus	Generator
4	G1	40	G11	116	G21
6	G2	43	G12	118	G22
9	G3	45	G13	138	G23
11	G4	47	G14	140	G24
13	G5	65	G15	144	G25
15	G6	70	G16	148	G26
18	G7	77	G17	149	G27
30	G8	79	G18	152	G28
35	G9	103	G19	162	G29
36	G10	112	G20		

A. WECC-179 bus test system

The detailed system parameters of WECC 179-bus test system are available in [4]. To facilitate the following representation, Table I rennumbers each generator bus.

1) *Scenario 1: Single FO source (Single oscillation frequency)* Taking generator G10 as the reference generator, a sinusoidal signal with an oscillation frequency of 0.37 Hz was continuously injected into the excitation system of G17 as an FO disturbance signal. The signal resonates with the intra-area oscillation mode with an oscillation frequency of 0.37 Hz.

Using the proposed time-frequency domain FOSL, the variations of active power, reactive power, frequency, and voltage amplitude logarithmic were calculated, respectively. The SWT coefficients matrix of the electrical increments was obtained using SWT via Eq. (7). The relative energy weight of electrical increments of each generator at each frequency was calculated using Eq. (9), and the results are shown in Fig. 2.

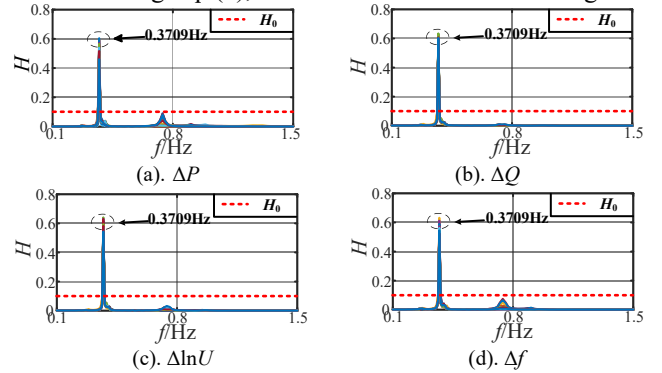


Fig. 2. Energy weights of the parameter increments of each generator at each frequency in scenario 1

It is obvious that the energy weights in the 0.3709 Hz frequency range for all generators are above the threshold H_0 , i.e., 0.1 Hz, indicating that the oscillation frequency of the FO mode is 0.3709 Hz. The SWT coefficients corresponding to the FO frequency are extracted from the SWT coefficient matrix. After the FO frequency is determined, the SWT coefficients at this frequency are used to calculate the SWT-based DEF in the time-frequency domain of the generators using (14). The results are shown in Fig. 3. It is observed that the SWT-based DEF of G17 is negative with a downward trend, indicating that G17 is injecting energy into the power grid, thus is the FO source. The SWT-based DEFs of the other generators are positive with an upward trend, indicating that they are FO sinks.

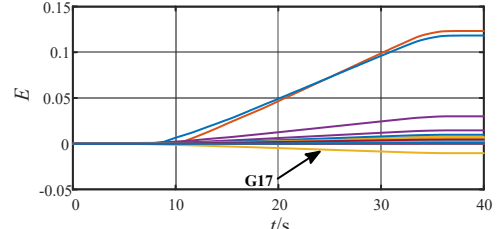


Fig. 3. SWT-based DEF of each generator in scenario 1

To further verify the accuracy of the proposed SWT-based DEF method, the SWT coefficients were used to reconstruct the time domain components with FO mode of electrical increments. These time domain components were then used to

calculate the time domain general DEF using (1), and the results are presented in Fig. 4. As can be observed, the general DEF of G17 exhibits a downward trend and continuously injects energy into the system, indicating that it is an FO source. On the other hand, the general DEFs of the remaining generators show an upward trend and continuously absorb energy from the system, indicating that they are FO sinks. These FOSL results using the general DEF method are consistent with the proposed SWT-based DEF results, which effectively confirms the high accuracy of the proposed method.

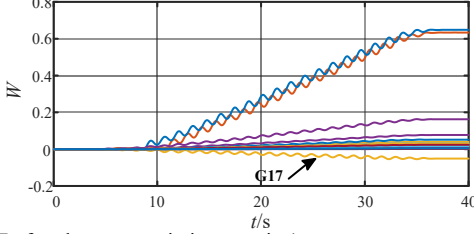


Fig. 4. DEF of each generator in in scenario 1

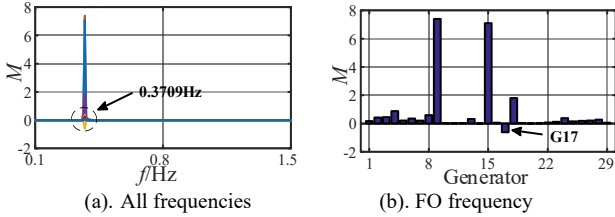


Fig. 5. SWT-based DES of each generator in scenario 1

Further, the SWT coefficient matrix of each electrical increment is substituted into (17) to calculate the SWT-based DES of generators, as shown in Fig. 5 (a). It can be observed that the SWT-based DESs of generators exhibit a peak or valley at 0.3709 Hz, which is consistent with the identified FO frequency using the proposed method. This peak/valley value is a clear indication of the presence of an FO mode with an oscillation frequency of 0.3709 Hz, as per the frequency domain FOSL criterion proposed in subsection III-B. It is worth noting that this frequency matches the oscillation frequency of the injected disturbance signal of 0.37 Hz, confirming the high accuracy of the proposed method in identifying the FO frequency. To locate the FO source in frequency domain, the SWT-based DESs at 0.3709 Hz is calculated and shown in Fig. 5 (b). It can be observed that the SWT-based DES of G17 is negative, indicating that G17 is the FO source. On the other hand, the SWT-based DESs of the remaining generators are positive, meaning that they are FO sinks. This result is consistent with the FOSL results obtained from the time-frequency domain analysis, which validates the effectiveness of the proposed method in locating the FO source.

In this section, a comprehensive comparison is conducted to further validate the accuracy of the proposed SWT-based DES method. The CWT-based DESs and FSST-based DESs are calculated, separately. These results are compared in Fig. 6. It can be observed from Fig. 6 (a) and Fig. 6 (c) that the CWT-based DESs and FSST-based DESs reach a peak/valley value at 0.3516 Hz and 0.3622 Hz, respectively. This indicates that the FO frequency of the system is determined to be 0.3516 Hz and 0.3622 Hz, which are different from the actual

injected disturbance frequency of 0.37 Hz with certain errors. As a result, it can be safely concluded that the proposed SWT-based DES method is more accurate than the CWT-based DES and FSST-based DES method in identifying the FO frequency.

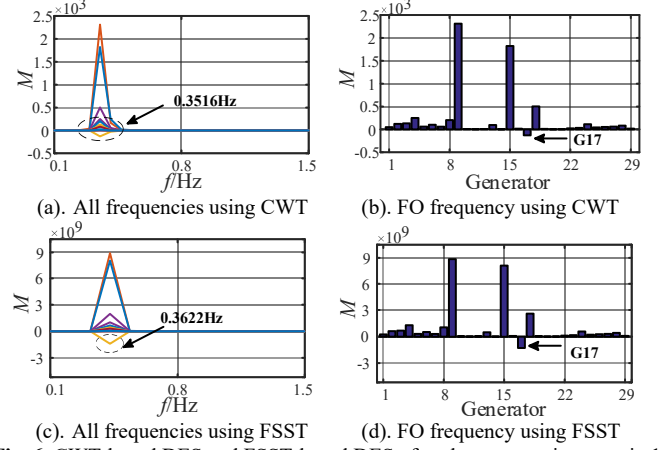


Fig. 6. CWT-based DES and FSST-based DES of each generator in scenario 1

2) *Scenario 2: Single FO source (Disturbance signal contains multiple harmonics)* In this scenario, the accuracy of the proposed FOSL method is tested when a disturbance signal containing multiple harmonics is injected continuously into the excitation system of G18. The disturbance signal is a periodic square wave signal with fundamental waves of 0.2 Hz and 0.6 Hz and multiple harmonics including 1 Hz and 1.4 Hz. Like scenario 1, the relative energy weights of each generator at each frequency are calculated using (9), and the results are presented in Fig. 7.

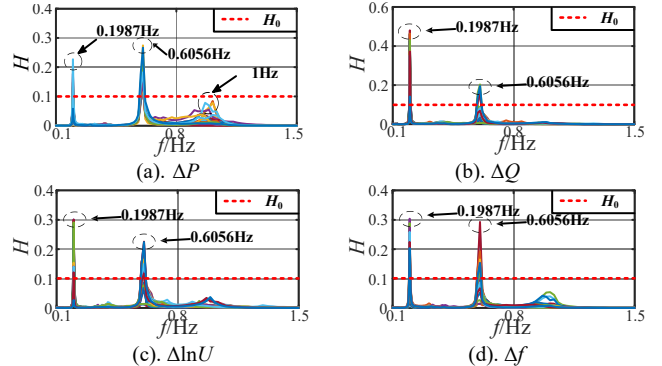


Fig. 7. Energy weights of parameter increments of each generator at each frequency in scenario 2

It can be observed from Fig. 7 that the oscillation frequencies of FO modes are 0.1987 Hz and 0.6056 Hz as the energy weights in the parameter increments at those frequencies exceed the threshold H_0 . Note that even though the injected disturbance signal includes higher harmonics like 1 Hz and 1.4 Hz, their amplitudes are relatively small and the damping of the corresponding natural oscillation mode of the system is favorable [4]. Consequently, they couldn't resonate with the power system natural oscillation mode, and the dominant FO frequencies are 0.1987 Hz and 0.6056 Hz. The frequency identification mentioned above is consistent with the result in [4], confirming the accuracy of the proposed method in identifying the dominant FO frequency.

Subsequently, employing the SWT coefficients at 0.1987 Hz and 0.6056 Hz, the SWT-based DEFs in time-frequency domain are calculated via (14), and the results are illustrated in Fig. 8. It is apparent that the SWT-based DEFs of G18 at 0.1987 Hz and 0.6056 Hz are negative with a downward trend. This trend signifies that G18 continuously injects energy into the power grid, categorizing it as an FO source.

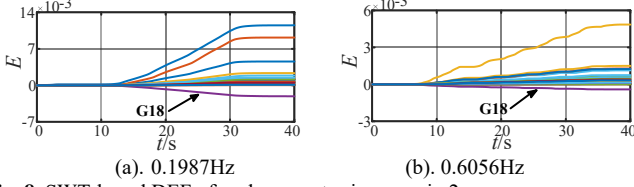


Fig. 8. SWT-based DEF of each generator in scenario 2

Fig. 9 shows the time domain general DEFs computed using (1). It can be observed that the general DEF of G18 shows a downward trend at 0.1987 Hz and 0.6056 Hz, indicating it is a FO source. The FOSL result of general DEF is consistent with the proposed SWT-based DEF, which effectively verifies the accuracy of the proposed method.

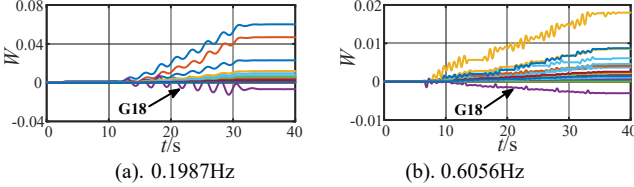


Fig. 9. DEF of each generator in scenario 2

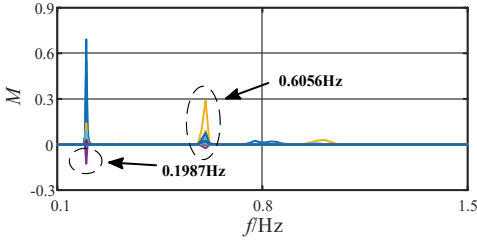


Fig. 10. SWT-based DES of each generator in scenario 2

The SWT-based DESs of generators are calculated via (17), and the results are shown in Fig. 10. It could be observed that the SWT-based DESs of the generators reach peak/valley values at 0.1987 Hz and 0.6056 Hz, respectively, indicating that the power system has two FO modes. Upon comparing the frequency of the injected disturbance signal, the FO frequencies of 0.1987 Hz and 0.6056 Hz identified by the proposed method are consistent with the injected disturbance frequencies of 0.2 Hz and 0.6 Hz, with errors of 0.65% and 0.93%, respectively. To further determine the FO source in the frequency domain, the SWT-based DESs of the generators at 0.1987 Hz and 0.6056 Hz are depicted in Fig. 11. As can be seen at 0.1987 Hz and 0.6056 Hz, the SWT-based DES of G18 is negative, indicating that it is a FO source. On the other hand, the SWT-based DESs of the rest generators are positive, suggesting that they are FO sinks.

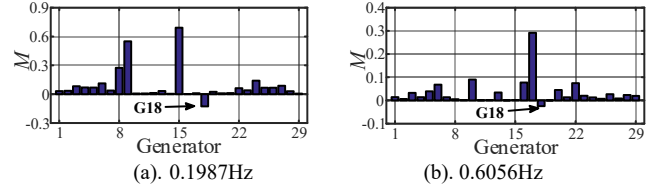


Fig. 11. SWT-based DES of each generator at FO frequency in scenario 2

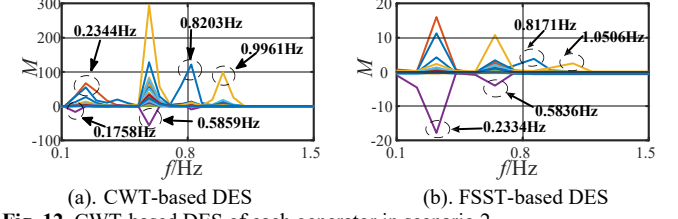


Fig. 12. CWT-based DES of each generator in scenario 2

To verify the accuracy of the proposed SWT-based DES method, the CWT-based DESs and FSST-based DESs are calculated, separately. The results are shown in Fig. 12. It is evident that the CWT-based DESs have peak/valley values at 0.1758 Hz, 0.2344 Hz, 0.5859 Hz, 0.8203 Hz, and 0.9961 Hz, respectively. It is worth noting that the CWT-based DES at 0.2 Hz is dispersed at 0.1758 Hz and 0.2344 Hz, and the CWT-based DES at 0.6 Hz is dispersed at 0.5859 Hz and 0.8203 Hz. This is because the CWT-based DES has a rather blurred representation, which causes a large deviation between the identified FO frequency and the actual one. The same situation also occurs in the FSST-based DES. To summarize, the results of the CWT-based DES and FSST-based DES are not consistent with the injected disturbance frequencies of 0.2 Hz and 0.6 Hz. By contrast, the proposed SWT-based DES method is more accurate and effective in locating the FO sources.

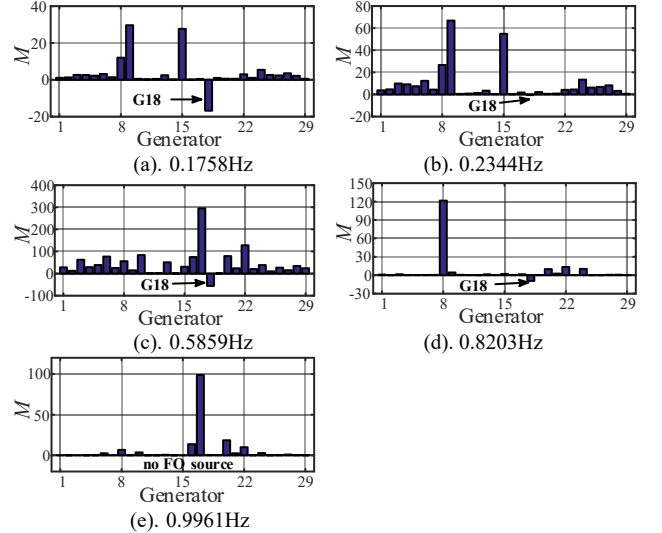


Fig. 13. CWT-based DES of each generator at FO frequency in scenario 2

Fig. 13 shows the CWT-based DESs of generators at 0.1758 Hz, 0.2344 Hz, 0.5859 Hz, 0.8203 Hz and 0.9961 Hz, respectively. It could be observed that the CWT-based DES effectively locates the FO source at 0.1758 Hz, 0.2344 Hz, 0.5859 Hz and 0.8203 Hz, but fails at 0.9961 Hz. As depicted in Fig. 10, Fig. 11, Fig. 12, and Fig. 13, the proposed

SWT-based DES method has higher resolution and stronger robustness in FOSL with multi-harmonics, allowing it to effectively identify the FO frequency and locate the FO source. In contrast, the CWT-based DES method has poor robustness and serious scale blurred representation, resulting in large errors in FO frequency identification and failure of FO source location.

3) *Scenario 3: Double FO sources* In this scenario, the accuracy of the proposed FOSL method in identifying multiple FO sources is demonstrated by injecting sinusoidal signals with oscillation frequencies at 0.65 Hz and 0.43 Hz continuously into the governing systems of G18 and G22, respectively.

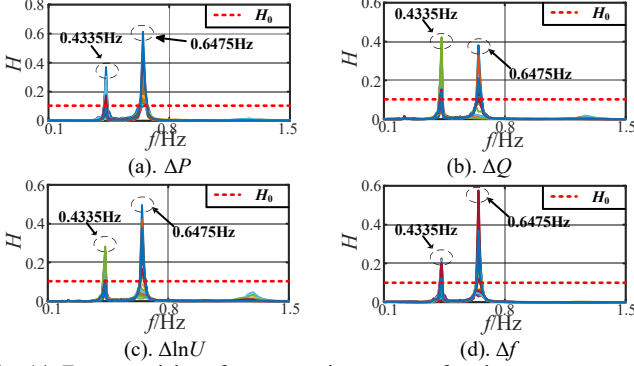


Fig. 14. Energy weights of parameter increments of each generator at each frequency in scenario 3

The energy weights of each generator at each frequency were calculated using (9), and the results are presented in Fig. 14. It can be observed that the energy weights at 0.4335 Hz and 0.6475 Hz of the parameter increments exceed the threshold H_0 , indicating that the FO frequencies are 0.4335 Hz and 0.6475 Hz. Subsequently, the DEFs in the time-frequency domain at 0.4335 Hz and 0.6475 Hz were calculated using the SWT-based method and shown in Fig. 15. Evidently, the SWT-based DEFs of G22 and G18 at 0.4335 Hz and 0.6475 Hz, respectively, are negative with a downward trend. This trend indicates that G22 and G18 are continuously injecting energy into the power grid. Thus, classifying them as the FO sources in this scenario.

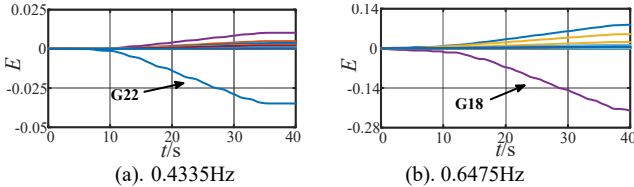


Fig. 15. SWT-based DEF of each generator in scenario 3

The SWT coefficients of electrical increments at 0.4335 Hz and 0.6475 Hz are utilized for reconstruction, and the time domain components associated with FO mode are derived. Following this, the general DEFs of generators are computed using (1), and the results are presented in Fig. 16. The general DEFs of G22 and G18 exhibit downward trends at 0.4335 Hz and 0.6475 Hz, confirming that they are FO sources. The FOSL result of general DEF is consistent with the proposed SWT-based DEF, thereby effectively verifying the location accuracy of the proposed method in double FO sources.

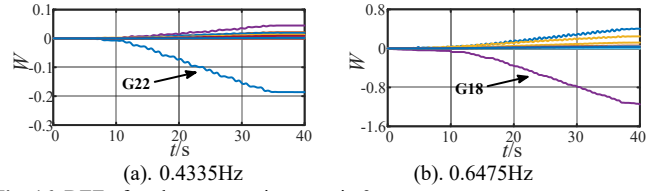


Fig. 16. DEF of each generator in scenario 3

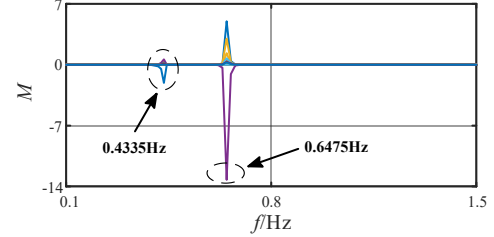


Fig. 17. SWT-based DESs of each generator in scenario 3

Furthermore, the SWT-based DESs of the generators are calculated via (17), and the results are presented in Fig. 17. It is observed that the SWT-based DESs of the generators exhibit peak/valley values at frequencies of 0.4335 Hz and 0.6475 Hz, respectively. These frequencies are consistent with the injected disturbance frequencies of 0.43 Hz and 0.65 Hz, with errors of 0.81% and 0.38%, respectively. As shown in Fig. 18, the SWT-based DESs of G22 and G18 are negative at 0.4335 Hz and 0.6475 Hz, confirming that they are FO sources, while the SWT-based DESs of the other generators are positive, indicating that they are FO sinks.

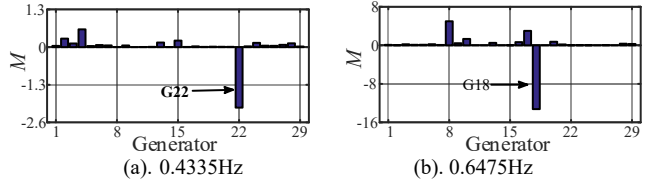


Fig. 18. SWT-based DES of each generator at FO frequency in scenario 3

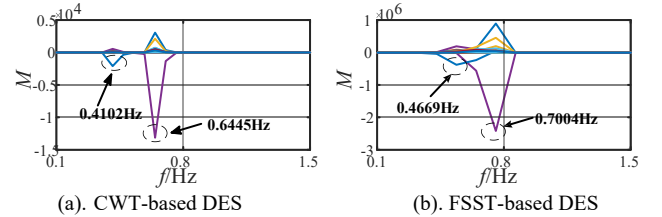


Fig. 19. CWT-based DES of each generator in scenario 3

Fig. 19 shows the CWT-based DESs and FSST-based DESs. The peak/valley values of the CWT-based DESs occur at 0.4102 Hz and 0.6445 Hz, respectively, while those in FSST-based DES are 0.4669 Hz and 0.7004 Hz. The errors between the identified frequencies and the injected disturbance frequencies are 4.6%, 0.85%, 8.58%, 7.75%, respectively. Nevertheless, considering FO frequency error analysis in the preceding paragraph, the proposed SWT-based DES method offers superior accuracy. Fig. 20 shows the CWT-based DESs of generators at 0.4102 Hz and 0.6445 Hz. It is observed that the CWT-based DESs of G22 and G18 are negative, which indicates that these two generators are the FO sources. This result effectively verifies the accuracy of the proposed FOSL method in identifying double FO sources.

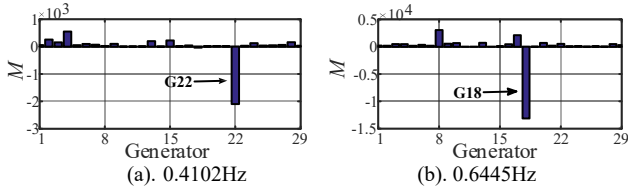


Fig. 20. CWT-based DES of each generator at FO frequencies in scenario 3

B. Measured PMU data of ISO New England

In this subsection, the effectiveness of the proposed FOSL method in actual power system is evaluated using PMU field measurements in the ISO New England. Specifically, on June 20th, 2019, an FO event with a frequency of 0.14 Hz occurred at the power plant radially connected by the line Ln:2. More PMU measured data can be found in [4].

Applying the proposed FOSL method, the variations of active power, reactive power, frequency, and voltage amplitude logarithmic were calculated and used to obtain the SWT coefficients matrix using (7). Subsequently, the relative energy weights of electrical increments at each frequency were computed using (9), and the results are presented in Fig. 21 for frequencies within [0.1 Hz, 0.7 Hz]. As shown in Fig. 21, the energy weights of the parameter increment at 0.1393 Hz exceeded the threshold H_0 , indicating that the FO mode frequency of the power system was 0.1393 Hz. Then, the SWT-based DEFs in the time-frequency domain at 0.1393 Hz were calculated using (14), and the results are shown in Fig. 22. The SWT-based DEF of the power plant radially connected by the line Ln:2 is negative and displays a downward trend, indicating that the power plant continuously injects energy into the power grid, and hence is an FO source. On the other hand, the SWT-based DEFs of the other power plants are positive and exhibit upward or unchanged trends, suggesting that they are FO sinks. As shown in [13] and [26], the time domain DEF results of Ln2 are non-monotonic, which makes it difficult to identify it as a FO source or sink. However, it is observed that the power plant radially connected by the line Ln:2 shows an overall decreasing trend throughout the entire time window with upward trends in some shorter windows. This FOSL result represents a significant improvement compared to the results in [13] and [26], making it easier to identify the FO source.

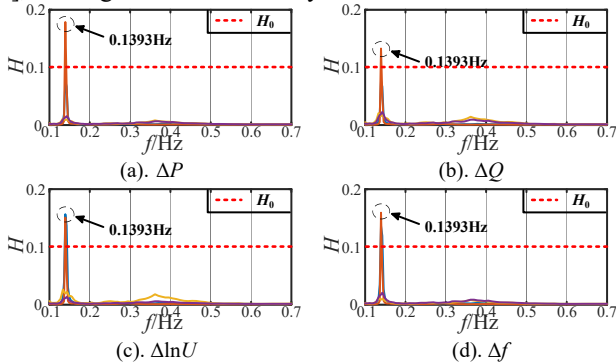


Fig. 21. Energy weights of the parameter increments of power plants at each frequency in ISO New England case

The proposed method of SWT-based DES in the frequency domain is applied by substituting the SWT coefficient matrix

of each electrical increment into (17) to calculate the SWT-based DES, and the results are shown in Fig. 23 (a). It is observed that the SWT-based DESs reach peak/valley values at 0.1393 Hz, indicating the FO frequency is 0.1393 Hz. Fig. 23 (b) shows the SWT-based DESs at 0.1393 Hz, it is observed that the SWT-based DES of the power plant radially connected by the line Ln:2 is negative, which indicates that it is an FO source. The SWT-based DESs of the other power plants are positive, which implies that they are FO sinks. The above results indicate that, compared to time-domain and time-frequency domain methods, the frequency-domain approach allows for an intuitive determination of the FO source based on the FOSL frequency-domain criterion proposed in this paper. This avoids the non-monotonic DEF results that can make it difficult to identify the FO source using time-domain methods.

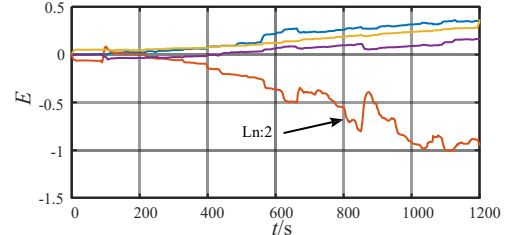


Fig. 22. SWT-based DEFs of each power plant in ISO New England

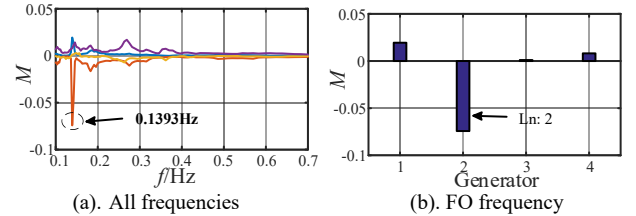


Fig. 23. SWT-based DES of each power plant in ISO New England

Fig. 24 displays the CWT-based DESs obtained using (15). As evident in Fig. 24(a), the CWT-based DES exhibits a peak/valley value at 0.1465Hz, indicating that the FO frequency is 0.1465Hz, with an error of 4.64% compared to the real FO frequency. Although both methods accurately locate the FO source, the proposed SWT-based DES method exhibits higher accuracy in identifying the FO frequency.

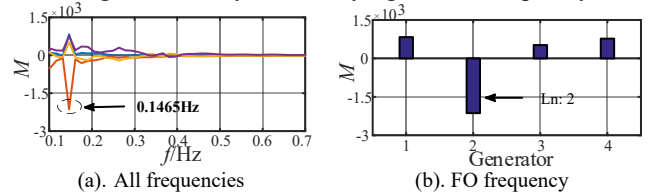


Fig. 24. CWT-based DES of each power plant in ISO New England

In conclusion, the results of the proposed FOSL methods in both time-frequency and frequency domains are consistent with the actual FO source, demonstrating their effectiveness and accuracy for actual power system FOSL. Further, the proposed SWT-based method showcases superior accuracy in identifying FO frequency, surpassing both CWT-based and FSST-based methods. These findings highlight the effectiveness and practicality of the proposed method in real-world system FOSL applications.

C. Comparison of computational efficiency

This subsection compares the computational efficiency of different FOSL methods, including SWT-based DES in frequency domain, SWT-based DEF in time-frequency domain, SWT-based DEF in time domain, CWT-based DES in frequency domain, CWT-based DEF in time-frequency domain, CWT-based DEF in time domain, MEMD-based DEF [19], and conventional DEF. The hardware configuration of the computing platform is CPU Intel Core i7-9750H with a main frequency of 2.6GHz and 16GB memory. Table II shows that the proposed SWT-based FOSL method in time-frequency and frequency domains are competitive in solution efficiency. It should be noted that, compared to the conventional DEF method, the approach proposed in this paper does offer some benefits, but these advantages come at a price in terms of computational time.

TABLE II

COMPUTATIONAL TIMES COMPARISON BETWEEN PROPOSED METHOD AND

OTHER EXISTING METHODS

Method	OTHER EXISTING METHODS			
	WECC-scenario 1/s	WECC-scenario 2/s	WECC-scenario 3/s	ISO New England
SWT frequency domain	12.184	11.427	12.392	12.035
SWT time-frequency domain	13.019	13.534	13.107	13.773
SWT time domain	14.654	14.392	14.301	15.011
CWT frequency domain	12.658	12.657	12.945	19.195
CWT time-frequency domain	13.855	13.642	13.878	21.159
CWT time domain	14.520	14.327	14.256	22.143
FSST frequency domain	12.769	12.022	12.945	13.056
MEMD	21.328	21.655	22.537	40.537
Conventional DEF	8.368	8.042	8.639	9.846

V. CONCLUSION

In this paper, an SWT-based time-frequency domain method and a frequency domain FOSL method are proposed. The expressions of the time-frequency domain DEF and the frequency domain DES are derived using the SWT, and the conventional time-domain DEF is extended to the time-frequency domain and frequency domain. The consistency of the dissipating energy in the time domain, time-frequency domain, and frequency domain is verified. The time-frequency domain and frequency domain-based FOSL using the information from WAMS is realized, offering a new perspective for the FOSL. Compared to the CWT-based method, the proposed method not only solves the inherent characteristics of CWT scale blurred representation, but also improves the accuracy of FO frequency identification and FOSL. Moreover, the proposed FOSL method can provide multi-dimensional FOSL information for power grid operators and provide a reference for the selection of subsequent oscillation suppression measures. Finally, the proposed methods are validated by the simulation data of the WECC-179 bus test system and the PMU measured data of the ISO New England.

APPENDIX

This appendix discusses the rationale behind selecting the relative energy weight threshold, H_0 , in this paper, based on

multiple sets of simulation data from the WECC 179-bus test system and field measurements gathered from the PMUs in ISO New England [4]. The values of H_0 are selected as 0.05, 0.1, and 0.15, respectively. Detailed data can be found in [4].

A. WECC-179 bus test system

Case1: In this case, a sinusoidal signal with a frequency of 0.86 Hz was continuously injected into the excitation system of generator G1 as a FO disturbance signal. The signal resonates with the local oscillation mode of the system with a frequency of 0.86 Hz. The proposed FOSL method was employed to calculate the increments of active power, reactive power, frequency, and logarithmic voltage amplitude, respectively. The SWT coefficients matrix of the electrical increments was obtained using SWT via Eq. (7). Subsequently, the relative energy weight of electrical increments at each frequency was calculated using Eq. (9), and the results are shown in Fig. A1.

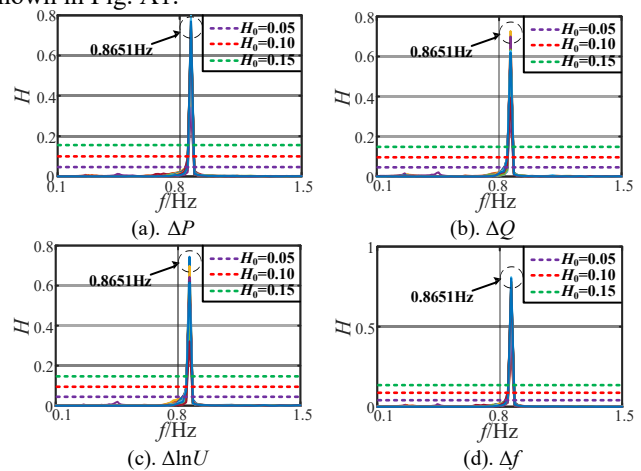
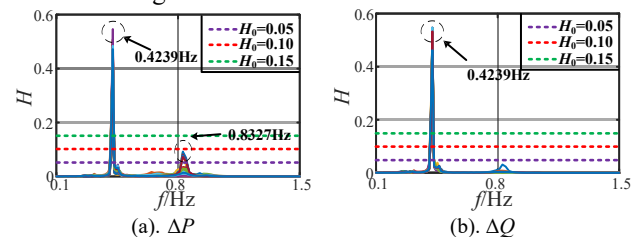


Fig.A1. Energy weights of the parameter increments of each generator at each frequency in case 1

In Case 1, it is evident that the increments for each generator exhibit their maximum relative energy weights at 0.8651 Hz. This observation suggests that the dominant FO frequency is 0.8651 Hz, and it can be reliably identified for all H_0 values (0.05, 0.1, and 0.15).

Case2: In this case, a sinusoidal signal with an oscillation frequency of 0.42 Hz was continuously injected into the excitation system of G18 as an FO disturbance signal. Using the proposed FOSL method, the increments of active power, reactive power, frequency, and voltage amplitude logarithmic were calculated, respectively. The SWT coefficients matrix of the electrical increments was obtained using SWT via Eq. (7). The relative energy weight of electrical increments at each frequency was then calculated using Eq. (9), and the results are shown in Fig. A2.



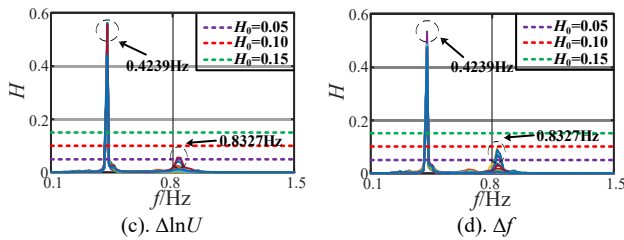


Fig.A2. Energy weights of the parameter increments of each generator at each frequency in case 2

In Case 2, it is evident that with a threshold H_0 of 0.05, the relative energy weights exceed the H_0 at frequencies 0.4239 Hz and 0.8327 Hz. However, upon comparing these frequencies with the injected disturbance frequency, it becomes evident that 0.8327 Hz is not the dominant FO frequency. This discrepancy is likely due to the frequency selection influenced by the relatively low magnitude of the H_0 . When H_0 is set to 0.1 and 0.15, only the frequency of 0.4239 Hz is designated as the FO frequency. This outcome aligns with the frequency of the injected disturbance.

B. Measured PMU data of ISO New England

Case3: On January 29th, 2018, an FO event with a frequency of 1.57 Hz occurred at the Gen2 power plant. Using the proposed FOSL method, the increments of active power, reactive power, frequency, and voltage amplitude logarithmic were calculated, respectively. The SWT coefficients matrix of the electrical increments was obtained using SWT via Eq. (7). The relative energy weight of electrical increments at each frequency was then calculated using Eq. (9), and the results are shown in Fig. A3.

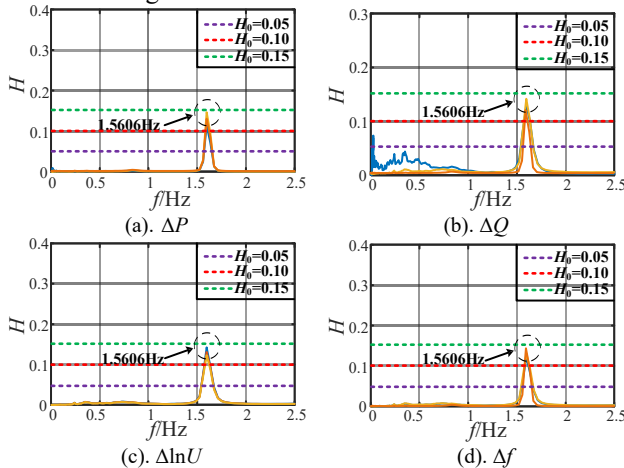


Fig.A3. Energy weights of the parameter increments of each power plant at each frequency in case 3

It is obvious that in Case 3, when the threshold is set to 0.15, there are no FO frequencies with relative energy weights higher than the threshold H_0 in all frequencies. This is likely due to the threshold H_0 being set too high, resulting in missing the FO mode. However, when the threshold H_0 is set to 0.1 and 0.05, the FO frequency of 1.5606 Hz is selected. This result aligns with the FO event.

Based on the analysis results from Fig. A1 to Fig. A3, the following conclusions can be drawn:

1) Setting the relative energy weight threshold H_0 too low may lead to inadvertent selection of non-FO modes from the measurements.

2) Conversely, when the relative energy weight threshold H_0 is set excessively high, FO modes might not be adequately identified.

3) The effective selection of the FO frequency without omitting dominant FO modes or incorporating irrelevant modes can be achieved by setting H_0 to 0.1 in all cases.

In summary, a rational and practical choice for the relative energy weight threshold H_0 in this study is 0.10, enabling the reliable identification of the FO frequency.

REFERENCES

- [1] B. Wang, K. Sun, "Location methods of oscillation sources in power systems: a survey," *J. Modern Power Syst. Clean Energy*, vol. 5, no. 2, pp. 151-159, March. 2017.
- [2] H. Ye, Y. Liu, P. Zhang, *et al*, "Analysis and detection of forced oscillation in power system," *IEEE Trans. Power Systems*, vol. 32, no. 2, pp. 1149-1160, March. 2017.
- [3] Y. Xu, C. Ma, X. Deng, *et al*, "Case of low-frequency oscillation induced by steam turbine valve control mode switchover and its mechanism analysis," *Electric power automation equipment*, vol. 35, no. 3, pp. 170-174, 2015.
- [4] [Online]. Available: <http://web.eecs.utk.edu/~kaisun/Oscillation/index.html>.
- [5] A. Singh, S. Ghosh and S. Banerjee, "Forced oscillation in Indian grid - case study," 2018 IEEE 7th International Conference on Power and Energy (PECon), Kuala Lumpur, Malaysia, 2018, pp. 117-122.
- [6] S. Chevalier, P. Vorobev and K. Turitsyn, "A Bayesian approach to forced oscillation source location given uncertain generator parameters," *IEEE Trans. Power Systems*, vol. 34, no. 2, pp. 1641-1649, March 2019.
- [7] X. Wang, K. Turitsyn, "Data-driven diagnostics of mechanism and source of sustained oscillations," *IEEE Trans. Power Systems*, vol. 31, no. 5, pp. 4036-4046, Sept. 2016.
- [8] S. Feng, B. Zheng, P. Jiang, *et al*, "A two-level forced oscillations source location method based on phasor and energy analysis," *IEEE Access*, vol. 6, pp. 44318-44327, 2018.
- [9] Y. Meng, Z. Yu, N. Lu, *et al*, "Time series classification for locating forced oscillation sources," *IEEE Trans. Smart Grid*, vol. 12, no. 2, pp. 1712-1721, March 2021.
- [10] S. Talukder, S. Liu, H. Wang and G. Zheng, "Low-frequency Forced Oscillation Source Location for Bulk Power Systems: A Deep Learning Approach," 2021 IEEE International Conference on Systems, Man, and Cybernetics (SMC), Melbourne, Australia, 2021, pp. 3499-3404.
- [11] L. Chen, Y. Min, W. Hu, "An energy-based method for location of power system oscillation source," *IEEE Trans. Power Systems*, vol. 28, no. 2, pp. 828-836, May. 2013.
- [12] P. G. Estevez, P. Marchi, C. Galarza, *et al*, "Complex dissipating energy flow method for forced oscillation source location," *IEEE Trans. Power Systems*, vol. 37, no. 5, pp. 4141-4144, Sept. 2022.
- [13] S. Maslennikov, E. Litvinov, "ISO New England experience in locating the source of oscillations online," *IEEE Trans. Power Systems*, vol. 36, no. 1, pp. 495-503, Jan. 2021.
- [14] S. Maslennikov, B. Wang, E. Litvinov, "Dissipating energy flow method for locating the source of sustained oscillations," *Int. J. Elect. Power Energy Syst.*, vol. 88, pp. 55-62, 2017.
- [15] Y. Cai, X. Wang, G. Joós and I. Kamwa, "An online data-driven method to locate forced oscillation sources from power plants based on sparse identification of nonlinear dynamics (SINDy)," *IEEE Trans. Power Systems*, vol. 38, no. 3, pp. 2085-2099, May 2023.
- [16] T. Jiang, H. Gao, X. Li, *et al*, "Forced oscillation source location in power system using dissipation energy spectrum," *Proceedings of the CSEE*, vol. 43, no. 8, pp. 2940-2953, Apr. 2023.
- [17] P. G. Estevez, P. Marchi, C. Galarza, *et al*, "Non-stationary power system forced oscillation analysis using synchrosqueezing transform," *IEEE Trans. Power Systems*, vol. 36, no. 2, pp. 1583-1593, March. 2021.
- [18] T. Jiang, M. Li, X. Li, *et al*, "Time-frequency Domain Location Method for Forced Oscillation Source in Power System," *Automation of*

- Electric Power Systems*, vol. 45, no. 9, pp. 98-106, May. 2021.
- [19] T. Jiang, B. Liu, X. Li, *et al*, "Forced oscillation location in power systems using multiple empirical mode decomposition," *Proceedings of the CSEE*, vol. 42, no. 22, pp. 8063-8074, Dec. 2022.
 - [20] L. Chen, M. Sun, Y. Min, *et al*, "Online monitoring of generator damping using dissipation energy flow computed from ambient data," *IET Gener. Transm. Distrib.*, vol. 11, no. 18, pp. 4430-4435, March 2017.
 - [21] X. Chu, Y. Yin, L. Gao, *et al*, "A new forced oscillation disturbance source location method based on empirical mode theory," *Proceedings of the CSEE*, vol. 34, no. 28, pp. 4906-4912, 2014.
 - [22] Daubechies I, Lu J, Wu H T, "Synchrosqueezed wavelet transforms: An empirical mode decomposition-like tool," *Applied and Computational Harmonic Analysis*, vol. 30, no. 2, pp. 243-261, 2011.
 - [23] S. Meignen, T. Oberlin, S. McLaughlin, "A new algorithm for multicomponent signals analysis based on synchrosqueezing: with an application to signal sampling and denoising," *IEEE Trans. Signal Processing*, vol. 60, no. 11, pp. 5787-5798, Nov. 2012.
 - [24] Mallat, S. G., "A Theory for Multiresolution Signal Decomposition: The Wavelet Representation," *IEEE Transactions on Pattern Analysis and Machine Intelligence*, vol. 11, no. 7, pp. 674-693, 1989.
 - [25] J. Bendat, A. Piersol, *Engineering applications of correlation and spectral analysis*, 2nd Ed., John Wiley & Sons, New York, 1993.
 - [26] D. Osipov, S. Konstantinopoulos and J. H. Chow, "A Cross-Power Spectral Density Method for Locating Oscillation Sources using Synchrophasor Measurements," in *IEEE Transactions on Power Systems*, doi: 10.1109/TPWRS.2022.3229255.